ELSEVIER

Journal of Structural Geology 28 (2006) 1261–1276

JOURNAL OF STRUCTURAL GEOLOGY

www.elsevier.com/locate/jsg

Constraining the relative strengths of high-grade metamorphic rocks using foliation refraction angles: an example from the Northern New England Appalachians

Wesley G. Groome *, Scott E. Johnson

Department of Earth Sciences, University of Maine, Orono, ME 04469, USA

Received 8 July 2005; received in revised form 8 March 2006; accepted 9 March 2006
Available online 11 May 2006

Abstract

Foliation refraction angles are used to estimate effective viscosity contrasts between metapelitic and metapsammitic layers in amphibolite-facies metaturbidites in the Presidential Range of the White Mountains, in eastern New Hampshire. An early-formed foliation, developed during km-scale nappe folding, consistently displays larger bedding-foliation angles in metapelitic units than metapsammitic units, suggesting that the metapelitic units had higher effective viscosities during this deformation. We collected bedding-foliation angle measurements from a combination of outcrops and locally-derived boulders to test the hypothesis that foliation refraction angles could be used to estimate the effective viscosity ratio between different rock types at high metamorphic grades. Our results show that the metapelitic layers were between 2 and 3 times more viscous than the metaspsammitic layers, which we attribute to the presence of large (up to 15 cm long), abundant (up to 30 vol.%) effectively rigid andalusite porphyroblasts in the metapelitic layers. We present a methodology for using foliation refraction angles to determine the effective viscosity ratios of different rock types, address the practical limitations we encountered, and suggest this method is an easy way of estimating the strength contrast between different rock types. Finally, we hypothesize that metamorphism resulting in porphyroblast growth can strengthen large crustal volumes during orogenesis.

Keywords: Foliation refraction; Metamorphic strengthening; New England Appalachians; Porphyroblasts; Rheology

1. Introduction

The mechanical structure of the crust controls strain partitioning during orogenesis, and can affect processes as diverse as the location of active metamorphism (e.g. Rubie, 1983; Brodie and Rutter, 1985; Koons et al., 1987; Bell and Hayward, 1991; Freuh-Green, 1994; Moecher and Wintsch, 1994; Bell et al., 2004), exhumation of deep-crustal rocks (e.g. Zeitler et al., 1993; Jamieson et al., 2002; Koons et al., 2002), and topographic evolution (e.g. Williams et al., 1994; Koons, 1995; Upton et al., 2003). Much of our knowledge about the rheology of mid-crustal rocks comes from: (1) extrapolation of experimental data on mineralogically simple rocks deformed under laboratory pressure, temperature and strain-rate conditions (e.g. Ji and Zhao, 1993; Kohlstedt et al., 1995; Farver and Yund, 1999, 2000; Hirth et al., 2001; Tenthorey and Cox, 2003); (2) geophysical observations (seismic, heat flow, geodedic measurements, etc.) from active orogenic belts, which can be used to constrain strain rates, geothermal gradients and the depth to the brittle–ductile transition (e.g. Chen and Molnar, 1983; Della Vedova et al., 1995; Carminati and Siletto, 1997; Holt et al., 2000; Maggi et al., 2000); and (3) the study of naturally-deformed rocks in ancient orogenic belts using field techniques to estimate strength contrasts between different rock types (e.g. Hudleston and Holst, 1984; Kanagawa, 1993; Dominic and McConnell, 1994; Hudleston and Lan, 1995; Gross et al., 1997; Treagus, 1999; Hippertt et al., 2001; Miller and Paterson, 2001; Urai et al., 2001; Treagus and Treagus, 2002; Kenis et al., 2004, 2005; Klepeis et al., 2004). Many of these techniques provide only snap-shots of the rheology of parts of the crust, and generally do not provide information about the temporal variability of rheology.

Metamorphism should alter the strength of rocks during orogenesis because metamorphic products may be stronger or weaker than the reactants (e.g. Poirier, 1982; Rubie, 1983, 1986; Brodie and Rutter, 1985, 1987; Koons et al., 1987;

* Corresponding author. Tel.: +207 581 2122; fax: +207 581 2202.
E-mail address: wesley.groome@umit.maine.edu (W.G. Groome).

0191-8141/$ - see front matter © 2006 Elsevier Ltd. All rights reserved.
doi:10.1016/j.jsg.2006.03.023

Tobisch et al., 1991; Freuh-Green, 1994; De Bresser et al., 2001; Stunitz and Tullis, 2001; Jamieson et al., 2002; Barnes et al., 2004; Keller et al., 2004). During orogenesis, zones of active metamorphism may be heterogeneously distributed within a given crustal volume, which would alter the strength of these volumes. If a crustal volume weakens during metamorphism, deformation will partition into that region, which can lead to rapid exhumation of mid- and lower-crustal rocks, which in turn can alter the thermal structure of shallower crustal levels (e.g. Brown and Solar, 1998; Handy et al., 2001; Jamieson et al., 2002; Koons et al., 2002). If a crustal volume strengthens during metamorphism, deformation will partition away from that region, which can catalyze metamorphic reactions elsewhere in the crust (e.g. Rubie, 1983; Brodie and Rutter, 1985; Koons et al., 1987; Freuh-Green, 1994; Bell et al., 2004).

Most studies of the effects of metamorphism on mid- and lower-crustal strength have concentrated on the effects of metamorphic weakening during the hydration of relatively anhydrous rocks or grain size reduction during dynamic recrystallization (e.g. Rubie, 1983, 1986; Brodie and Rutter, 1985, 1987; Koons et al., 1987; Stunitz and Tullis, 2001). Few studies have addressed the strengthening effects of prograde metamorphism either resulting from metamorphic dehydration or the growth of relatively strong minerals (e.g. Jin et al., 2001; Moore and Saffer, 2001; Steffen et al., 2001; Hacker et al., 2003). In this study, we document the strengthening of metapelitic layers relative to metapsammitic layers in amphibolite-facies metaturbidites. We suggest that this strength contrast was the result of growth of abundant, large andalusite porphyroblasts in the pelitic layers. We further hypothesize that this strengthening would lead to transient orogen-scale strain partitioning, which may in turn catalyze metamorphism in other parts of the middle crust, leading to strengthening over a large area.

2. The rheology of polymineralic rocks: theoretical approaches

In this paper, we consider 'strength' to broadly be a measure of the resistance to deformation of a rock unit, which may be expressed as a yield stress (σ_1–σ_3) for plastic deformation, viscosity or effective viscosity ($\sigma/\dot{\varepsilon}$) for viscous deformation (either Newtonian or non-Newtonian) or the elastic modulus (σ/ε) for elastic deformation. In general, a strong rock is one that has a high resistance to deformation and a weak rock is one that has a low resistance to deformation. The strength of polymineralic rocks is generally viewed in terms of the relative strengths, volume fraction and distribution of constituent minerals (e.g. Jordan, 1988; Handy, 1990; Tullis et al., 1991; Ji and Xia, 2002; Treagus, 2002; Ji, 2004; Johnson et al., 2004) (Fig. 1). Two theoretical end-member bounds describing the strength of a polymineralic rock have been proposed, one assuming that the strain-rate, and by extension the finite strain, is the same in all phases (Voigt Bound) and one assuming that the differential stress experienced by all phases is the same (Reuss Bound) (see Appendix A for the mathematical derivation of these limiting cases). Most treatments of the rheology of natural polyphase materials assume that strength trends fall between the two theoretical end-members, with aggregates consisting of strong inclusions in a weak matrix following a 'Reuss-type' bound and those consisting of weak inclusions in a strong matrix following a 'Voigt-type' bound (e.g. Handy, 1990; Tullis et al., 1991; Bons and Urai, 1994; Ji and Xia, 2002), although there is a general consensus that these bounds do not adequately describe the strength of polymineralic rocks except at low abundance of either strong or weak phase (see, for example, Ji et al., 2001). Appendix A presents the mathematical derivation of the Voigt and Reuss bounds as well as the other strength trends on Fig. 1.

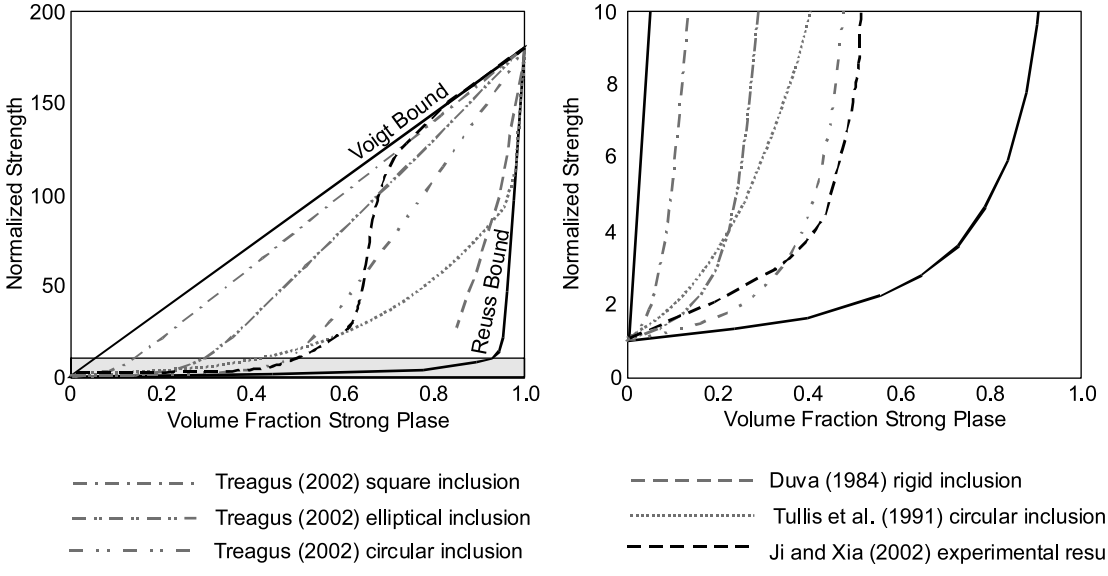

Fig. 1. Graph illustrating the Voigt and Reuss bounds as well as models of Treagus (2002), Tullis et al. (1991) and Duva (1984) and experimental results reported in Ji and Xia (2002) for the effects of increasing volume fractions of a strong phase on the strength of a two-phase aggregate. All values are normalized to the strength of the weak phase.

Natural experiments on the strength of two-phase aggregates generally record a transition between 'Reuss-type' and 'Voigt-type' bounds at inclusion abundance between approximately 40 and 60% (e.g. Arzi, 1978; Jordan, 1987; Shea and Kronnenburg, 1993; Ji et al., 2001; Ji and Xia, 2002; Takeda and Obata, 2003). The divergence from the limiting bounds as an aggregate approaches the critical volume fraction of inclusion (~40%) is largely a function of the strength contrast between the inclusion and the matrix, such that large strength contrasts will cause significant changes in strength at inclusion fractions as low as 25% (e.g. Arzi, 1978; Ji et al., 2001; Ji and Xia, 2002). Therefore, if the porphyroblasts are significantly stronger than the bulk matrix, porphyroblastic rocks should be significantly stronger than porphyroblast-free rocks at intermediate porphyroblast volume fraction (on the order of 25%), and the general strength evolution will diverge from a 'Reuss-type' bounding limit (e.g. Groome et al., in press).

In nature, phyllosilicate-rich pelitic layers in turbidite couplets are considered to be weak because they generally record higher finite strains (e.g. Treagus, 1983, 1988, 1999, and references therein). Based on foliation refraction measurements from sedimentary and low-grade metasedimentary rocks, Treagus (1999) estimated that psammitic units have between 2 and 10 times higher effective viscosities than pelitic units and Kenis et al. (2004, 2005) estimated that pelitic units had effective viscosities approximately 2–5 times lower than psammitic units based on mullion shape measurements. Experimental deformation of mica-rich rocks suggests that micas are weak, when sheared parallel to {001}, relative to quartz at low temperatures (e.g. Shea and Kronnenburg, 1993; Tullis and Wenk, 1994), and numerical models (e.g. Johnson et al., 2004) suggest that rocks experience significant weakening when mica grains become interconnected to form a foliation. These observations suggest that the relative weakness of low-grade, phyllosilicate-rich, pelitic rock is due at least in part to the weakness of mica.

In general, prograde metamorphism of pelitic rocks results in a decrease in the volume fraction of weak hydrous minerals, such as clays, and a corresponding increase in relatively strong anhydrous minerals, such as garnet (e.g. Bucher and Frey, 1994). In many cases, the volume fraction of strong porphyroblastic minerals (i.e. staurolite, garnet, andalusite, kyanite) can be quite high, which should significantly alter the strength of these rocks. If the volume fraction of effectively rigid porphyroblasts increases sufficiently, metapelitic layers should become stronger than interlayered metapsammitic layers, which typically have inappropriate bulk compositions for the growth of porphyroblastic phases (Fig. 1).

3. Extracting rheological information from naturally-deformed rocks

The relative strengths of naturally-deformed rocks can be estimated using several field techniques, including: (1) differences in strain between deformed clasts and matrix (e.g. Gay, 1968a,b, 1976; Lisle et al., 1983; Treagus and Treagus, 2002), (2) boudinage wavelength to thickness ratios (e.g. Smith, 1975, 1977), (3) fold wavelength to thickness ratios (e.g. Smith, 1975, 1977), (4) fold shape (e.g. Chapple, 1968, 1969; Fletcher, 1979; Hudleston and Holst, 1984), (5) differences in fracture density (e.g. Shackleton et al., 2005), (6) mullion lobe shape (e.g. Urai et al., 2001; Kenis et al., 2004, 2005), and (7) foliation refraction angles (e.g. Treagus, 1983, 1988, 1999). By using these techniques a mechanical stratigraphy for a rock succession can be constructed for a particular crustal section (e.g. Miller and Paterson, 2001; Klepeis et al., 2004). In this study, we use foliation refraction measurements to estimate the relative strengths of the metapelitic and metapsammitic layers in amphibolite facies metaturbidites.

3.1. Theoretical basis for using foliation refraction

The refraction of foliation surfaces at contacts between rocks with different effective viscosities is a well documented phenomenon (e.g. Dieterich, 1969; Roberts and Stromgard, 1972; Hobbs et al., 1982; Treagus, 1983, 1988, 1999; Kanagawa, 1993; Sengupta, 1997; Talbot, 1999; Hippertt et al., 2001; Lagoeiro et al., 2003; Viola and Mancktelow, 2005) (Fig. 2A). The use of foliation refraction angles to estimate effective viscosity contrasts between adjacent rock types is based on the premise that the ratio of the finite shear strain ($\gamma = \tan\psi$) in two rock types (A and B) with different effective viscosities (η_A and η_B) is proportional to the viscosity contrast between the rock types (e.g. Treagus, 1999):

$$\frac{\gamma_A}{\gamma_B} = \frac{\tan\psi_A}{\tan\psi_B} = \frac{\eta_B}{\eta_A} \quad (1)$$

In an ideal case, one would endeavor to measure the orientation of a feature that was originally perpendicular to the viscosity contact (such as a burrow in a sandstone) to assess the shear strain in each layer. However, these features are rare in metamorphic rocks.

Regardless of whether a foliation plane tracks the X–Y plane of the finite strain ellipsoid (e.g. Treagus, 1983, 1988, 1999) or is a material plane rotated during progressive non-coaxial deformation (e.g. Hobbs et al., 1982; Henderson et al., 1986; Viola and Mancktelow, 2005), foliation-bedding angles can be used to estimate the effective viscosity contrast between adjacent rock types. If a foliation develops essentially perpendicular to bedding early in a deformation and rotates as a material surface during progressive deformation, then foliation would represent an original line perpendicular to a viscosity contact (i.e. bedding) and can be used as a strain marker (Fig. 2B). However, using geometric arguments, Treagus (1999) suggested that the difference between the orientation of a rotated material surface and the X–Y plane of the finite strain ellipsoid is virtually indistinguishable if the stretch ratio ($R \approx X/Z$) of the finite strain ellipse is greater than approximately 5, which is a typical value for folded slates (e.g. Treagus, 1999, and references therein).

Fig. 2C illustrates the assertions made above. In a two-dimensional plane strain analysis, an arbitrary line (L), which

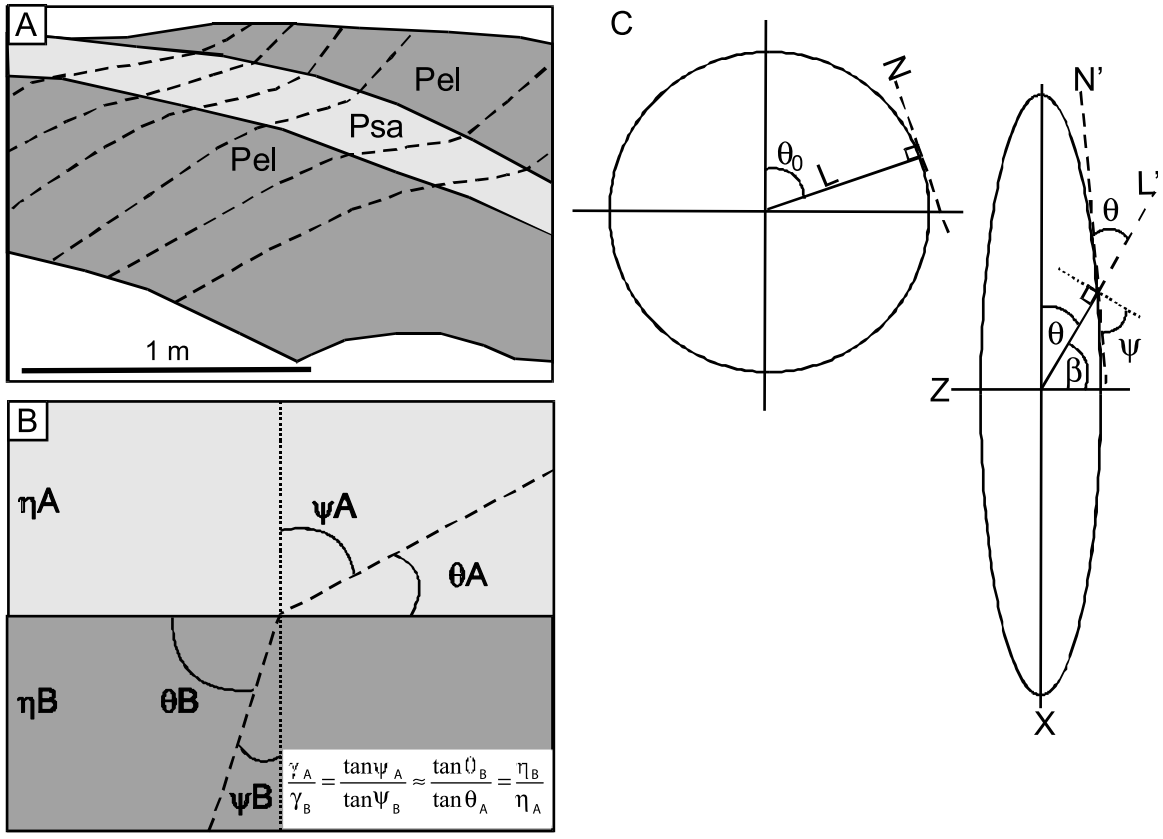

Fig. 2. (A) Sketch from Mt. Washington showing refracting foliations at the contact between metapelite (Pel) and metapsammite (Psa). The larger bedding-foliation angle in the metapelitic layer suggests this layer had a higher effective viscosity than the metapsammitic layer. (B) Schematic diagram illustrating the relationship between shear (ψ), bedding-foliation angles (θ) and relative viscosities (η) for a two-layered system (modified from Treagus, 1999). (C) Undeformed and deformed two-dimensional strain ellipses illustrating the relationship between the rotation of an arbitrary line (L) and its normal (N), angular shear (ψ), the angle (θ) between the line and the X-axis of the ellipse and the angle (β) (modified from Treagus, 1999).

could be bedding or some other viscosity contrast, and a marker perpendicular to it (N) will rotate antithetically during deformation. The shear strain (γ) is measured by taking the tangent of the angle (ψ) between the deformed normal line (N′) and a line perpendicular to the deformed viscosity contrast line (L′):

$$\gamma = \tan\psi \tag{2}$$

It can be shown (Treagus, 1999) that the angle ψ is less than 5° different from the angle β between the axis of finite shortening (Z) and the deformed viscosity contrast line orientation (L′) at stretch ratios greater than approximately 5, such that:

$$\tan\beta \approx \tan\psi = \gamma \tag{3}$$

where β is complementary to θ, the angle between the direction of maximum finite extension (X) and the deformed viscosity contrast line (L′) (Fig. 2C), such that:

$$\beta = 90 - \theta \approx \psi = 90 - \theta' \tag{4}$$

Thus, the angle between L′ and the X-axis of the strain ellipsoid is approximately equal to the angle between N′ and L′. Substituting this relationship into Eq. (1) yields:

$$\frac{\gamma_A}{\gamma_B} = \frac{\tan\psi_A}{\tan\psi_B} \approx \frac{\tan\beta_A}{\tan\beta_B} = \frac{\tan\theta_B}{\tan\theta_A} = \frac{\eta_B}{\eta_A} \tag{5}$$

which relates the shear strain ratio (γ_A/γ_B) and the viscosity ratio (η_B/η_A) to the ratio of the bedding-foliation angles ($\tan\theta_B/\tan\theta_A$) in each layer (Treagus, 1999).

4. Presidential Range geology

The Presidential Range of eastern New Hampshire is located near the western margin of the Central Maine Basin, a variably deformed and metamorphosed Paleozoic lithotectonic unit extending from Massachusetts to New Brunswick (e.g. Bradley, 1983; Van Staal et al., 1998; Bradley et al., 2000; Tucker et al., 2001) (Fig. 3). The stratigraphy of the Presidential Range consists predominantly of the Rangeley Sequence, which, from oldest to youngest, consists of the Silurian Rangeley, Smalls Falls, Madrid, Perry Mountain and the Devonian Littleton formations (e.g. Hatch et al., 1983; Wall, 1988; Allen, 1992; Eusden et al., 1996). This succession is polymetamorphic with an early regional metamorphism in the andalusite stability field overprinted by a later regional metamorphism in the sillimanite stability field

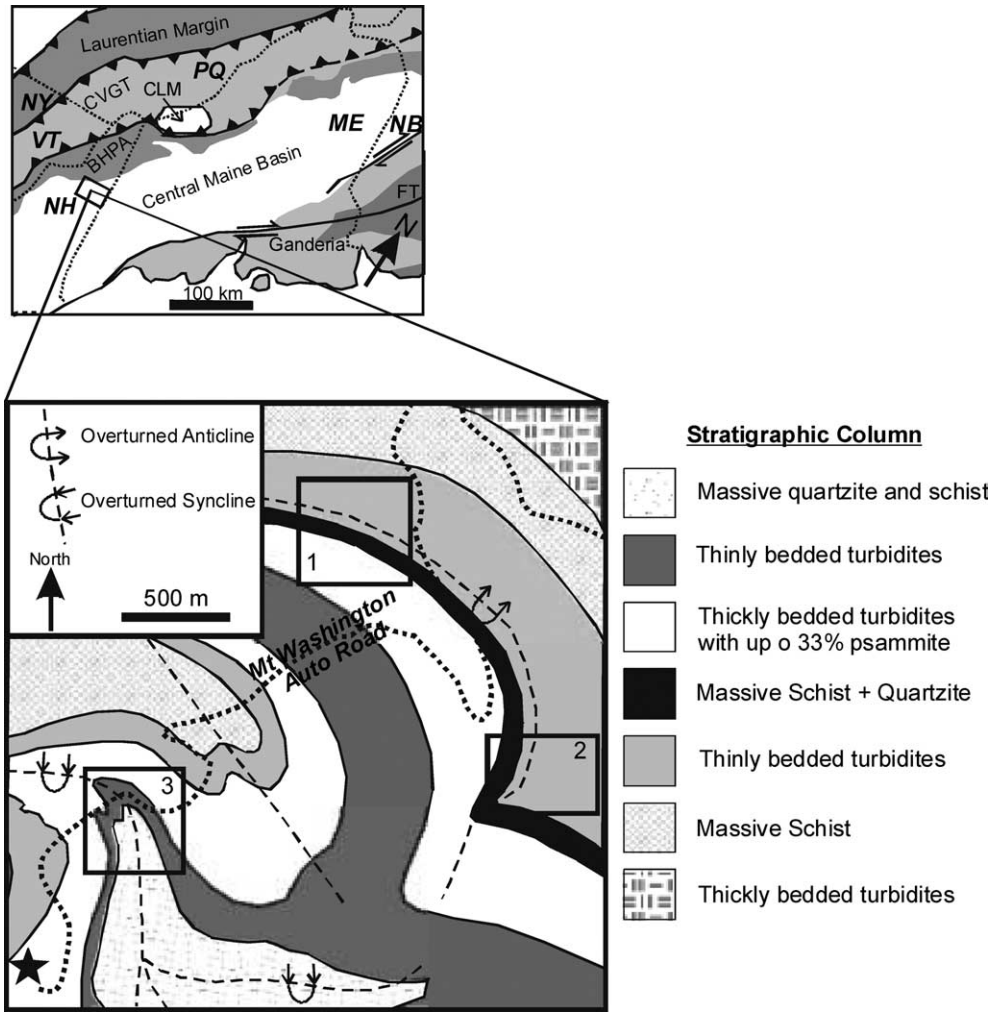

Fig. 3. Location map and detailed geologic map of the eastern flank of Mt. Washington (modified from Van Staal et al., 1998; Eusden et al., 1996). CVGT = Connecticut Valley, Gaspe Trough; BHPA = Bronson Hill, Piscataquis Arc; FT = Fredricton Trough; CLM = Chain Lakes Massif. The boxes numbered 1, 2 and 3 outline the detailed study areas discussed in this paper.

(e.g. Wall, 1988; Eusden et al., 1996). Early andalusite-grade metamorphism resulted in the growth of abundant, large andalusite porphyroblasts that commonly form interlocking networks of elongate porphyroblasts in pelitic layers (Fig. 4A). This metasedimentary succession is intruded by several syn-tectonic Devonian granitoid plutons and a post-tectonic two-mica granite of Carboniferous age (e.g. Hatch et al., 1983; Eusden et al., 2000).

Regional mapping has identified up to five phases of deformation in the Presidential Range region (Eusden et al., 1996). D_1 resulted in km-scale recumbent isoclinal east-verging folds. This was followed by a localized thrusting event, D_2, which juxtaposed gneissic rocks with schistose rocks in the Clay Klippe (Eusden et al., 1996). After thrusting, a period of folding, D_3, produced localized, small amplitude open folds with east–west-trending fold axes. Later east- and west-verging, asymmetric, open 100-m-scale folding, D_4, was followed by the development of a localized crenulation cleavage, D_5. Two regionally extensive planar fabrics are recognized in the Presidential Range: S_1 is an early, penetrative, axial planar foliation associated with the km-scale east-verging folds and S_4 is a later axially planar crenulation associated with the 100-m-scale asymmetric folds. Of the five deformations observed in the field, only D_1 was a high strain event (shortenings on the order of 75%). The second highest strain event (D_4) resulted in shortening on the order of only 10–15% (Kugel, 2004; Rodda, 2005), thus the deformation history of the study area can be viewed as a single, penetrative high strain deformation overprinted by several lower strain, localized deformations.

This study was undertaken in the hinge zones of two early F_1 isoclinal folds on the slopes of Mt. Washington, which were not significantly affected by later deformation (D_2 through D_5) (Fig. 3). The area investigated consists of thinly to thickly bedded turbidite couplets of the Littleton Formation. Bedding is on the order of a few centimeters to a meter thick, with metapelite layers tending to be thicker than metapsammite layers. Both sharp and gradational contacts between metapelitic and metapsammitic beds are commonly observed within individual turbidite couplets. In this region, the early-formed axial planar foliation (S_1) refracts into the pelitic layers, with bedding-foliation angles being greater in these layers than in metapsammitic layers (Fig. 4B and C). In addition, the three

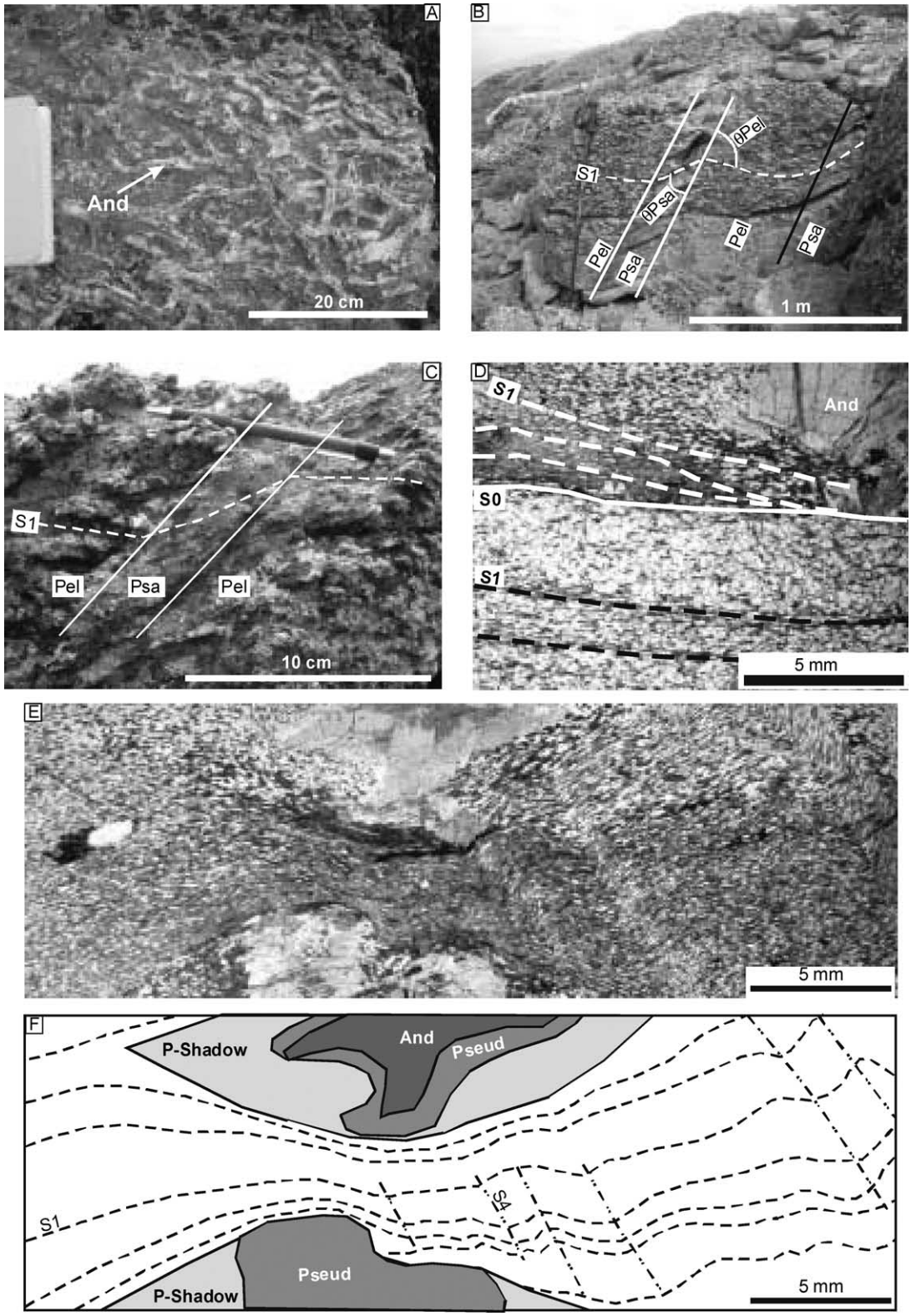

Fig. 4. (A) Photograph of a typical metapelitic layer in the study area, showing the high abundance of andalusite porphyroblasts (And), which are pseudomorphed to coarse-grained muscovite, blocky sillimanite and fibrolitic sillimanite. Note the interlocking elongate porphyroblasts. (B) Photograph from Mt. Washington showing the refracting of foliation (S_1) at the bedding contact between metapelitic (Pel) and metapsammitic (Psa) layers in a turbidite bed. The bedding-foliation angles (θ_{Pel} and θ_{Psa}) are also shown. (C) Close-up photograph of refracting foliation at a bedding contact showing that foliation can be traced without disruption from one layer to the next, suggesting that there was minimal slip along the bedding surface. (D) Photomicrograph of a contact between metapelite (top) and metapsammite (bottom) showing the development of the S_1 foliation in the two layers. And = andalusite. (E) Photomicrograph of a metapelitic layer from the limb of an early nappe fold (plane polarized light). S_1 is bedding parallel in this section. The foliation wraps around the andalusite porphyroblasts, suggesting that they were present in the rock during the formation of this foliation. Also note the presence of late staurolite porphyroblasts that post-date S_1. (F) Sketch of the photomicrograph in (E) showing the orientations of S_0, S_1 and S_4 as well as the wrapping of S_1 around the porphyroblasts.

detailed study sites chosen for this project did not show evidence for significant later deformation, which would have obscured the S_1 refraction morphology (Fig. 4D–F).

The presence of anastamosing S_1 foliation traces around andalusite porphyroblasts and the development of pressure shadows around the porphyroblasts suggest that this foliation was either post- or synchronous with andalusite growth (Fig. 4E and F) (e.g. Passchier and Trouw, 1996; Johnson, 1999; Vernon, 2004). The presence of an earlier bedding-parallel foliation cannot be ruled out based on our observations, but if a bedding-parallel foliation was present prior to D_1 folding and the development of S_1, it would probably have contributed to the layer anisotropy present in the stratigraphic layering during folding, and would not fundamentally affect the theoretical basis for using foliation refraction angles to estimate effective viscosity contrasts.

5. Estimating the effective viscosity contrast between metapelitic and metapsammitic layers

5.1. Methodology

Foliation refraction angles were measured on a variety of outcrops and locally-derived boulders in the study area (Fig. 4A). Each set of measurements consisted of a bedding orientation and the foliation orientation in the different layers. Measurements for this study were only taken along the sharp contact between the metapsammitic and metapelitic layers at the base of turbidite couplets. Along the sharp contact, the difference in foliation orientation between the metapelitic and metapsammitic beds is greatest (i.e. $\tan\theta_{Pel}$:$\tan\theta_{Psa}$ is the greatest), therefore by recording our measurements along these contacts we calculate a *maximum* effective viscosity contrast between the two rock types. Several sites were investigated where the foliation gradually changed orientation in the gradational part of the turbidite couplets, indicating a gradual change in relative viscosity, but these locations were not used to estimate effective viscosity ratios. The gradually-reoriented foliation in these gradational contacts corresponds with a marked decrease in porphyroblast abundance, a corresponding increase in quartz and feldspar abundance, and we attribute the gradual re-orientation of foliation to changes in porphyroblast abundance and modal mineralogy in general.

Bedding-foliation angles for the metapsammitic and metapelitic layers were measured using a lower-hemisphere, equal-angle projection of the poles to bedding and foliation (Fig. 5). The angle between the pole to bedding and the pole to the foliation in the two different layers was measured and used as the angle between bedding and foliation. The effective viscosity ratios were calculated for each measurement using Eq. (6):

$$\frac{\tan\theta_{Pel}}{\tan\theta_{Psa}} = \frac{\eta_{Pel}}{\eta_{Psa}} \tag{6}$$

where θ is the angle between bedding and the foliation in the unit indicated, Pel is the metapelitic layer, Psa is the metapsammitic layer and η is the effective viscosity of a given layer.

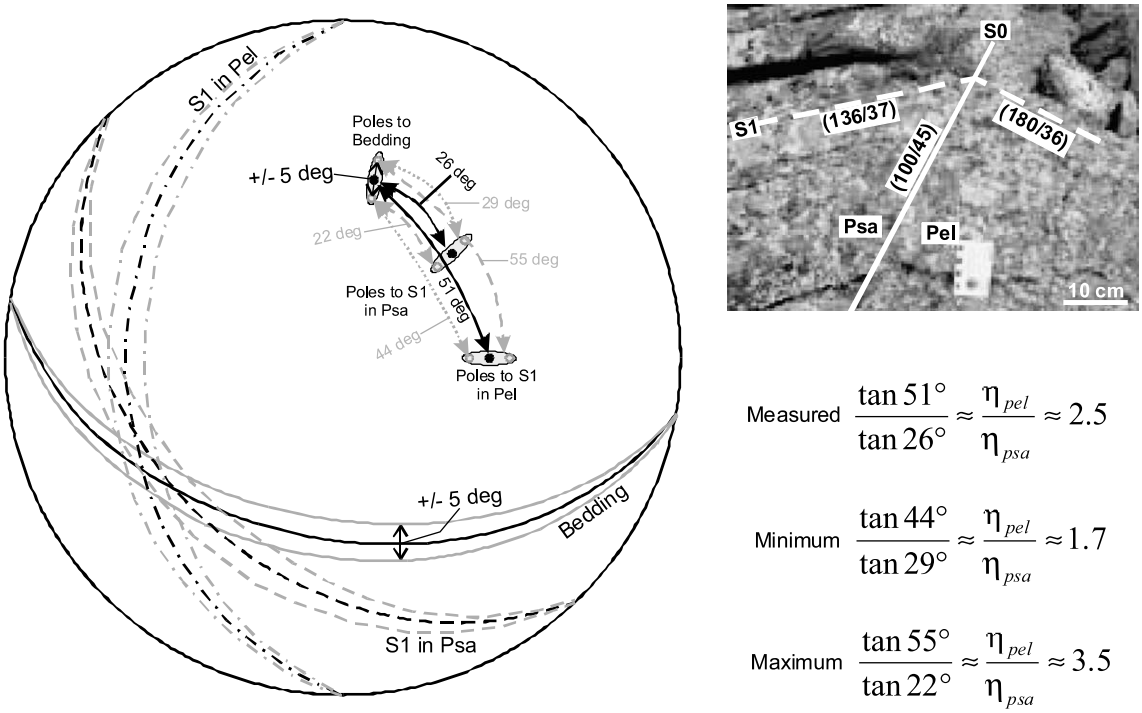

Fig. 5. Example of the method used in this paper. (Right) Field photograph of refracting foliation at the bedding contact. The orientations of bedding and foliation are given using right-hand rule convention. (Left) Lower-hemispheric, equal area projection of the orientation of bedding and foliation showing how the angles between bedding and foliation were determined, as well as the incorporation of a $\pm 5^\circ$ error. Using Eq. (6), the effective viscosity contrast (η_{Pel}/η_{Psa}) in this example is approximately 2.5.

Three study sites, located in the hinge zones of two F_1 folds, were chosen for the systematic collection of orientations (Fig. 3). These sites were chosen because: (1) outcrops and locally-derived boulders did not show evidence of later deformation, which may have affected the viscosity estimations; (2) the sites were well exposed and contained abundant locally-derived boulders; and (3) the sites traversed the mapped hinge zones, going from one limb through to the other so refraction angles could be studied on either side of the fold hinges.

We justify the use of measurements from locally-derived boulders because our technique does not require a spatial relationship to bedrock structure. Owing to extensive frost heave in the study area, the majority of the measurements were made on boulders showing moderate displacements from bedrock. Boulders displaying a wide range of bedding-foliation angles were investigated, ranging from nearly bedding-parallel to nearly bedding-orthogonal. This spread in orientations was deliberately sought out so that samples from various parts of the fold hinge zones could be measured to determine if the effective viscosity ratios estimated by the foliation refraction method would remain consistent as the angles changed in different parts of the fold. In the hinge zone of the fold, bedding-foliation angles should be large, whereas in the limbs bedding-foliation angles should be small (Fig. 6). If Eq. (6) is valid for estimating effective viscosity ratios, it should not matter where in the fold the measurements are taken because the bedding-foliation angles should change in a systematic way through the fold hinge.

Each set of measurements was plotted on a lower-hemisphere, equal-angle projection and the angle between bedding and foliation for each bed was measured using the poles to bedding and foliation (Fig. 5). The computer program StereoWin (Allmendinger, 2002) was used for the equal-angle plots as well as for measuring the angles between the poles. A total error of $\pm 5°$ was assigned to each measurement, accounting for systematic and random compass errors and human error in measurement. Using these errors, we were able to determine the maximum and minimum angles between bedding and foliation and calculate the range of relative viscosity values from our data set. Furthermore, we discarded any measurements that plotted with bedding-metapelite foliation and bedding-metapsammite foliation intersection lineations more than 30° apart. Ideally, the intersection lineations from each bed should be exactly the same, and for the most part they are within 5° in our data set. However, in some instances where either bedding or foliation is gently dipping, small errors in measurement can lead to slightly larger errors in the coincidence of intersection lineations.

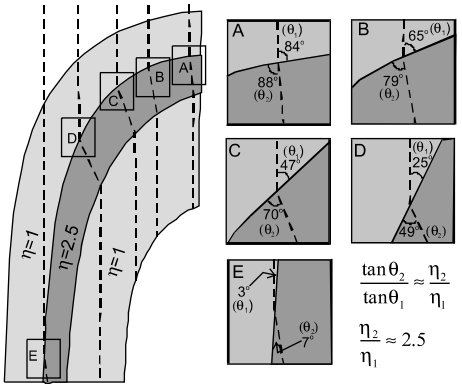

Fig. 6. Idealized fold profile showing how bedding-foliation angles change from fold hinge to fold limb. The ratios of the bedding-foliation angles remain constant from hinge to limb, with a viscosity contrast of 2.5 between the layers.

Discrepancies in the orientation of bedding-foliation intersection lineations from one bed to the next could result from a re-orientation of bedding or foliation during subsequent deformation. However, we avoided taking bedding-foliation measurements in locations where there was obvious evidence for subsequent deformation, such as a prominent crenulation cleavage, for just this reason. Furthermore, estimates of shortening during late deformation suggest that the maximum amount of shortening associated with late folding was on the order of 15% (e.g. Kugel, 2004; Rodda, 2005), which should not have significantly affected the bedding-foliation angles related to the early folding. For these reasons, we are confident that our bedding-foliation angle determinations provide a reasonable estimate for the effective viscosity contrasts between metapelitic and metapsammitic units.

5.2. Results

A total of 77 measurements were used in this study (Table 1). The calculated effective viscosity ratios from throughout the study area have a mean η_{Pel}:η_{Psa} of 2.39 with a standard deviation of 1.32 (Fig. 7A). From the raw data calculations, there are six measurements with $\eta_{Pel} < \eta_{Psa}$, but the remaining 71 (92% of the data) return values greater than 1, suggesting that the porphyroblast-rich metapelitic units were consistently stronger than the metapsammitic units. A plot of the distribution of maximum and minimum viscosity limits (i.e. the values calculated using the maximum and minimum angles between bedding and foliation, respectively) (Fig. 7B) shows that even by including a measurement error of $\pm 5°$, the majority of the viscosity calculations have $\eta_{Pel} > \eta_{Psa}$, further supporting our conclusion that the porphyroblast-rich metapelitic units had higher effective viscosities than the metapsammitic units. The average viscosity ratio for all data (measured + maximum/minimum calculations) is 3.53 with a standard deviation of 4.7; however, when values in excess of the 95th percentile (greater than 14) and less than the 5th percentile (less than 0.24) are excluded, the total average is 2.66 (standard deviation = 2.26). This is in close agreement with the average for values calculated from the measured data alone (2.39), thus we conclude that the porphyroblast-rich metapelitic units were on the order of 2–3 times more viscous than the porphyroblast-free metapsammitic units. The practical limitations of our methodology are discussed below.

Table 1
Field measurements and relative viscosity ratios determined using Eq. (6)

Field data							Errors				Viscosity range	
Site[a]	S_0[b]	S_1 (Ps)[b]	S_1 (Pe)[b]	Ps–S_0	Pe–S_0	η_{Pel}:η_{Psa}[c]	Ps–S_0 (Max)	Ps–S_0 (Min)	Pe–S_0 (Max)	Pe–S_0 (Min)	Min	Max
1	182.18	51.41	53.44	54	58	1.16	63	46	66	48	1.07	2.17
1	098.37	087.14	293.10	25	46	2.22	34	14	57	36	1.08	6.18
1	355.63	005.84	309.69	24	42	2.02	33	14	45	40	1.29	4.01
1	175.30	149.37	138.33	16	20	1.27	23	13	23	16	0.81	1.84
1	287.36	323.17	096.18	24	54	3.09	32	17	64	43	1.49	6.71
1	316.61	002.62	032.71	41	71	3.34	43	38	73	67	2.53	4.19
1	137.44	087.42	054.37	33	50	1.84	38	30	57	45	1.28	2.67
1	286.37	323.29	044.40	21	65	5.59	24	18	73	56	3.33	10.07
1	233.19	032.01	083.14	20	33	1.78	29	12	41	23	0.77	4.09
1	314.43	342.53	337.47	24	18	0.73	29	21	22	15	0.48	1.05
1	309.48	319.27	169.03	21	51	3.22	32	12	60	41	1.39	8.15
1	300.31	343.26	096.14	21	43	2.43	24	17	54	34	1.51	4.50
1	265.64	097.22	084.31	81	87	3.02	85	75	89	84	0.83	15.35
1	092.36	266.13	269.34	50	73	2.74	59	39	80	60	1.04	7.00
1	321.80	350.63	012.34	32	60	2.77	38	28	68	54	1.76	4.65
1	100.45	136.37	180.36	26	51	2.53	29	22	55	44	1.74	3.53
1	078.78	019.17	305.42	69	73	1.26	77	62	77	67	0.80	2.30
1	081.59	270.54	282.21	67	79	2.18	77	57	88	68	0.57	18.60
1	025.63	276.76	272.61	81	85	1.81	82	79	86	84	1.34	2.78
1	079.51	348.11	247.14	52	64	1.60	58	46	75	55	0.89	3.60
1	281.70	298.57	321.34	21	46	2.70	27	18	55	39	1.59	4.40
1	239.38	197.16	123.12	28	45	1.88	37	21	53	37	1.00	3.46
1	080.64	286.54	286.23	68	85	4.62	78	57	89	84	2.02	37.20
1	227.73	208.78	189.84	18	39	2.49	24	16	43	36	1.63	3.25
1	276.54	294.42	333.35	19	43	2.71	25	13	47	38	1.68	4.64
1	262.29	312.31	315.46	24	35	1.57	27	21	41	32	1.23	2.26
1	104.76	120.79	141.72	16	36	2.53	25	15	38	34	1.45	2.92
1	272.47	253.18	050.24	31	65	3.57	40	21	75	57	1.84	9.72
1	180.88	275.25	275.25	90	90	1.00	86	85	85	86	0.80	1.25
1	169.71	109.41	070.56	56	86	9.65	61	53	88	81	3.50	21.58
1	064.33	077.48	009.54	20	42	2.47	27	10	49	38	1.53	6.52
1	192.80	152.45	121.59	48	68	2.23	57	42	72	66	1.46	3.42
1	328.50	353.53	016.32	21	36	1.89	18	23	31	41	1.42	2.68
1	280.51	311.67	316.56	31	29	0.92	29	36	27	32	0.86	1.43
1	086.76	007.62	332.40	74	85	3.27	70	77	80	88	1.31	10.42
1	293.68	324.64	337.33	29	49	2.08	27	33	40	55	1.29	2.80
1	307.65	014.47	047.21	57	70	1.78	53	60	64	79	1.18	3.88
1	277.54	351.22	171.04	51	55	1.16	46	57	48	62	1.07	1.82
1	274.66	285.37	302.50	30	29	0.96	21	39	24	34	0.55	1.76
1	043.44	323.47	248.56	54	84	6.91	49	60	73	87	1.89	16.59
1	287.60	216.21	084.39	56	82	4.80	50	63	72	88	1.57	24.03
1	308.54	271.18	015.20	41	49	1.32	32	49	43	55	0.81	2.29
2	72.66	197.47	173.77	83	85	1.40	76	88	82	89	0.25	14.28
2	239.14	164.31	156.71	30	68	4.20	35	25	75	65	3.06	8.00
2	232.78	218.74	218.74			1.00	18	13	13	18	0.71	1.41
2	350.27	20.38	32.50	20	35	1.92	26	16	40	28	1.09	2.93
3	110.30	28.44	347.45	48	66	2.02	54	42	73	56	1.08	3.63
3	96.58	266.03	003.11	59	64	1.23	72	50	67	54	0.45	1.98
3	321.63	222.47	194.39	78	88	6.09	83	72	89	81	0.78	18.61
3	93.66	354.34	307.35	76	85	2.85	80	66	86	74	0.61	6.37
3	126.59	57.11	18.41	54	75	2.71	63	49	84	70	1.40	8.27
3	163.16	245.16	295.25	21	37	1.96	27	14	43	28	1.04	3.74
3	064.32	163.41	193.60	54	82	5.17	61	47	88	73	1.81	26.70
3	102.82	100.26	90.15	57	68	1.61	65	45	76	57	0.72	4.01
3	242.22	271.29	300.42	13	34	2.92	21	11	40	31	1.57	4.32
3	095.48	021.07	279.24	47	73	3.05	53	41	83	63	1.48	9.37
3	256.20	344.31	327.41	37	40	1.11	42	29	44	34	0.75	1.74
3	050.90	090.30	090.30			1.00	62	71	71	62	0.65	1.54
3	029.48	292.15	203.07	51	55	1.16	57	45	66	45	1.00	2.25

(*continued on next page*)

Table 1 (*continued*)

Field data							Errors				Viscosity range	
Site[a]	S_0[b]	S_1 (Ps)[b]	S_1 (Pe)[b]	Ps–S_0	Pe–S_0	η_{Pel}:η_{Psa}[c]	Ps–S_0 (Max)	Ps–S_0 (Min)	Pe–S_0 (Max)	Pe–S_0 (Min)	Min	Max
3	081.08	174.08	241.30	12	38	3.68	18	4	48	27	1.57	15.88
3	081.64	036.22	229.16	48	75	3.36	57	43	87	68	1.61	20.46
3	164.14	345.16	009.54	30	67	4.08	40	20	76	57	1.84	11.02
3	175.33	243.38	284.60	37	73	4.34	43	33	84	70	2.95	14.65
3	214.32	186.18	143.10	20	31	1.65	26	17	36	25	0.96	2.38
3	91.30	169.44	18.33	44	35	0.73	40	51	31	41	0.49	1.04
3	164.64	30.54	92.65	75	64	0.55	68	83	60	67	0.21	0.95
3	218.65	303.21	097.08	64	69	1.27	60	71	61	77	0.62	2.50
3	250.27	224.22	289.12	11	19	1.77	19	9	27	14	0.72	3.22
3	246.14	093.32	063.47	47	60	1.62	35	54	51	71	0.90	4.15
3	007.21	332.35	344.67	21	47	2.79	17	30	39	58	1.40	5.23
3	106.64	121.27	200.44	40	72	3.67	28	47	68	79	2.31	9.68
3	181.66	318.63	267.66	65	77	2.02	59	73	73	80	1.00	3.41
3	270.47	051.62	073.44	81	88	4.54	71	87	79	89	3.00	19.73
3	142.08	034.14	340.64	18	72	9.47	10	26	60	81	3.55	35.81
3	145.31	093.22	354.28	23	55	3.36	20	28	47	66	2.02	6.17
3	55.86	239.15	107.40	80	64	0.34	67	84	60	71	0.18	1.23
3	036.30	351.16	174.04	22	32	1.55	18	28	25	42	0.88	2.77

Statistics: average viscosity ratio = 2.39; standard seviation = 1.32

[a] Refer to Fig. 3 for location.

[b] Strike, dip (dip is to the right).

[c] Viscosity ratio calculated using Eq. (6).

6. Discussion

6.1. Practical limitations

In our application of foliation refraction angles to estimate effective viscosity ratios, we recognize three main limiting conditions as follows:

(1) Small errors in field measurements propagate through the analysis and can cause large errors in the effective viscosity ratio; therefore, the position in the fold where the measurements are taken is important with positions showing the smallest bedding-foliation angle leading to the largest errors. As an example, consider Fig. 8, which shows two hypothetical conditions, one in which the bedding-foliation angles are large and one in which the angles are small. Fig. 8A shows a situation with low bedding-foliation angles in both beds. When the $\pm 5°$ error is incorporated in the viscosity estimation, the spread in relative viscosity is 1.2–6.3 (η_{Pel}:η_{Psa}). The lower estimate

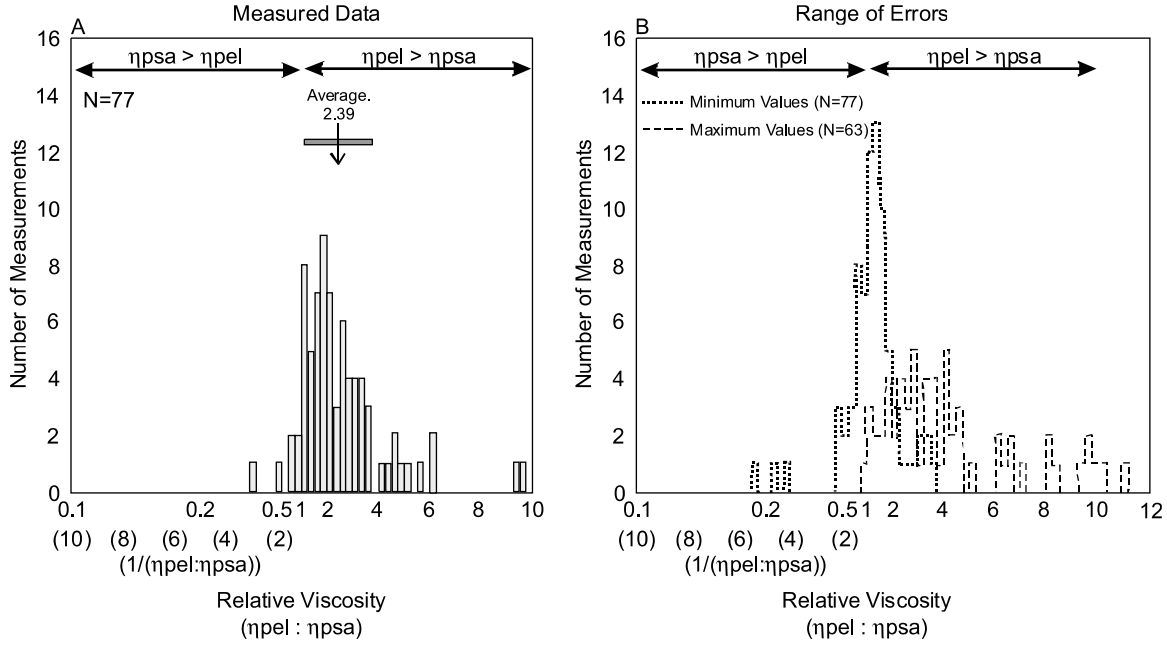

Fig. 7. (A) Histogram of the calculated effective viscosity ratios (η_{Pel}:η_{Psa}) based on the field measurements. The mean of 2.39 is indicated, and the scale bar represents the 1σ error. (B) Histogram of calculated effective viscosity ratios based on the maximum and minimum bedding-foliation angles based on the $\pm 5°$ error.

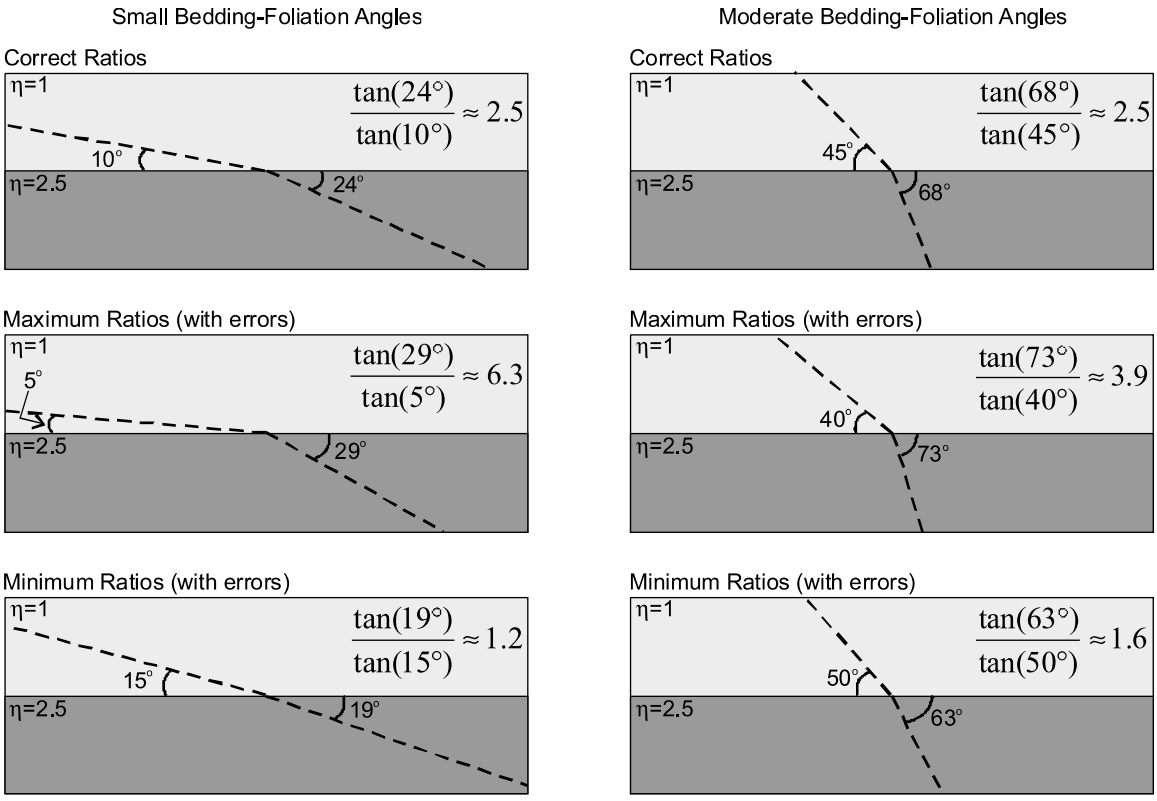

Fig. 8. Example illustrating the effects of where in the fold profile measurements are taken. (A) Bedding-foliation angles were measured on the limb of a fold where the angles are small. When a $\pm 5^\circ$ error is incorporated into the measurement, the spread in viscosity contrasts is relatively large (1.2–6.3). (B) Bedding-foliation angles were measured in the hinge zone of a fold, where the angles are large. Incorporating the $\pm 5^\circ$ error results in less spread of viscosity contrast values (1.6–3.9).

is 0.48 times the measured effective viscosity ratio, whereas the upper estimate is 2.5 times the actual effective viscosity ratio of 2.5. Fig. 8B shows the situation where the bedding-foliation angle is large. When the $\pm 5^\circ$ error is incorporated in this situation, the spread in effective viscosity ratios is 1.6–3.9. The lower estimate is 0.64 times the actual effective viscosity ratio, whereas the upper estimate is 1.5 times the actual ratio.

(2) Continuity from one bed to another is required if the foliation refraction angles are to be used to estimate effective viscosity ratios (e.g. Treagus, 1999). If significant layer-parallel slip is accommodated at bedding interfaces, then large strains could be partitioned into these interfaces, and foliation refraction angles would only provide a minimum estimate for viscosity contrasts. In our field example, we found no compelling evidence for localization of layer-parallel slip along thin interfaces during the folding. In all of the samples we investigated, foliation planes could be traced from one layer to another with continuity (Fig. 4D).

(3) Measurements should only be taken along sharp contacts between different rock types. The refraction of foliation at sharp contacts between different rock types should be the greatest; therefore these measurements will allow one to calculate the *maximum* effective viscosity contrast. Differences in finite strain through a single bed, either resulting from gradual changes in effective viscosity or differences in tangential longitudinal strain, could lead to gradually re-oriented foliations within a single bed, as seen in many of our gradational contacts between metapelitic and metapsammitic units. Therefore, we conclude that only foliation measurements taken along sharp contacts between units can be used to calculate effective viscosity ratios.

6.2. Broader implications

The strengthening of metapelitic layers during porphyroblast growth will lead to overall strengthening of the crustal volume experiencing porphyroblast-producing metamorphic reactions. In a layered stratigraphic succession, such as in the Presidential Range, as the metapelitic layers strengthen during porphyroblast growth, more strain will partition into the metapsammitic layers. The degree to which the stratigraphic succession strengthens as a whole is strongly dependent on the initial effective viscosity contrast between metapelitic and metapsammitic layers. Published effective viscosity contrasts between metapsammitic and porphyroblast-free metapelitic layers (η_{Psa}:η_{Pel}) range from 2 to 10 (e.g. Treagus, 1999; Kenis et al., 2004, 2005). If porphryoblastic metapelitic layers are between 1.5 and 2 times stronger than metaspsammitic layers, as in our case, the stratigraphic succession as a whole would have strengthened by a factor of 2–10 as strain partitions into the formerly strong metapsammitic layers.

In our study area, andalusite schists outcrop over at least a 5×10 km area, and may have been more extensive prior to subsequent metamorphic overprinting. During andalusite-grade

metamorphism, this entire area would have been strong relative to surrounding areas that did not experience these metamorphic reactions. This should have led to deformation partitioning around this area until subsequent metamorphic weakening during migmatization. This hypothesis is consistent with observations that later deformation in the Presidential Range area resulted in much lower strain than F_1, except in zones that were weakened during subsequent migmatization.

The strain partitioning around this strong crustal volume may have helped catalyze subsequent metamorphic reactions in relatively weak zones peripheral to it. The andalusite schists are surrounded by rocks that were migmatized during overprinting sillimanite grade metamorphism (e.g. Wall, 1988; Allen, 1992). The partitioning of deformation into the relatively weak areas around the Presidential Range area may have catalyzed partial melting reactions by allowing enhanced fluid flow in these zones, which would have lowered the solidus of metapelitic rocks (e.g. Patino Duce and Johnston, 1991; Gardien et al., 1995; Johnson et al., 2001). Oxygen isotope data from White Mountains migmatites suggests that partial melting may have been fluxed by external fluid flow through these rocks (Allen, 1992). Once partial melting commenced in the migmatite zones, further strain partitioning into these zones would likely have occurred (e.g. Hollister and Crawford, 1986; Brown and Solar, 1998), which would have led to low strains being recorded in andalusite schists during syn-melting deformation.

The presence of a large, strong mid-crustal zone may have also changed the topographic evolution of the New England Appalachians during the Acadian Orogeny, which would have affected factors such as sediment budgets for associated basins, local paleoclimate in the Devonian, and localized exhumation of high grade metamorphic rocks (e.g. Koons, 1989, 1995; Koons et al., 2002; Upton et al., 2003). The few studies investigating the relationship between mid-crustal rheology and the surface evolution of orogenic belts (e.g. Molnar and Tapponnier, 1981; Williams et al., 1994; Koons, 1995; Carminati and Siletto, 1997; Petrini et al., 2001; Upton et al., 2003) suggest that their broad-scale topographic evolution is coupled to mid-crustal rheology. The topographic profile of an orogen is a first-order control on the local climate (e.g. Koons, 1989, 1995), which in turn can lead to climate-enhanced exhumation of high-grade metamorphic rocks, altering the geothermal gradient in an orogen (e.g. Kuhni and Pfiffner, 2001; Schlunegger and Hinderer, 2001; Koons et al., 2002), and affecting sediment budgets in peripheral basins (e.g. Willet et al., 2003; DeCelles, 2004; Panien et al., 2005). The strengthening of a large volume of the middle crust during prograde metamorphism would inevitably affect all of these tectonic processes.

7. Conclusions

Based on our field study, the following conclusions can be made:

(1) Statistically-consistent ratios of bedding-foliation angles in metapelitic and metapsammitic layers in amphibolite-facies metaturbidites indicate that foliation refraction measurements can be used to estimate effective viscosity ratios in high-grade metamorphic rocks.
(2) Larger bedding-foliation angles in andalusite-rich metapelitic units suggest that the metapelitic units had higher effective viscosities than porphyroblast-free metapsammitic units. This effective viscosity relationship is the opposite of what is recorded in lower-grade, porphyroblast-free rocks (e.g. Treagus, 1999) and we hypothesize that the effective viscosity reversal in our rocks is due to the presence of effectively rigid andalusite porphyroblasts in the metapelitic units.
(3) Porphyroblast-rich rocks are common in many orogenic belts, and we hypothesize that metamorphic strengthening is a common phenomenon during orogenesis. The strengthening of large crustal volumes (on the order of 1000s km^3) during metamorphism will affect the geodynamic evolution of orogenic belts, and is investigated further in Groome et al. (in press).

Acknowledgements

Funding for this project came from NSF Grant # EAR 0207717 (to SEJ) and from the Geological Society of America Grants in Aid Program (to WGG). We are grateful to Dyk Eusden for introducing us to the geology of the Presidential Range area, Malissa Washburn for field assistance, and the US Forest Service Androscoggin Ranger District, the Appalachian Mountain Club and the Mount Washington Auto Road for logistical support. Sue Treagus, Peter Koons, Marty Yates, Chris Gerbi and Erwin Melis provided constructive criticism on early drafts. Journal reviews by Holger Stunitz and Christoph Hilgers improved the quality of this manuscript.

Appendix A. Derivation of two-phase aggregate mathematical expressions plotted on Fig. 1

Two end-member mathematical relationships have been used relating the bulk strength of a two phase material (σ_c) to the volume fraction of the constituent phases (V_{strong} and V_{weak}) and the relative strengths of the phases (σ_{strong} and σ_{weak}) (e.g. Takeda, 1998; Ji and Xia, 2002; Takeda and Obata, 2003):

$$\sigma_c = V_{strong}\sigma_{strong} + (1 - V_{strong})\sigma_{weak} \quad \text{(A1)}$$

$$\dot{\varepsilon}_c = V_{strong}\dot{\varepsilon}_{strong} + (1 - V_{strong})\dot{\varepsilon}_{weak} \quad \text{(A2)}$$

Eq. (A1) (Voight Bound) assumes that the strain rate for each phase (and the bulk strain) is the same and that the bulk strength (σ_c) of a polyphase material increases linearly with increasing volume fraction (V_{strong}) of the strong phase (e.g. Ji and Xia, 2002). Eq. (A2) (Reuss Bound) assumes that all phases are subjected to a constant differential stress and that

the bulk strain rate ($\dot{\varepsilon}_c$) is a function of the strain rate in each phase ($\dot{\varepsilon}_{strong}, \dot{\varepsilon}_{weak}$) (e.g. Ji and Xia, 2002).

By simplifying the rheologic model to a linear viscous model ($\eta = (\sigma/\dot{\varepsilon})$), Eq. (A2) can be re-written as:

$$\sigma_c = \left(\frac{\phi_s}{\sigma_s} + \frac{\phi_w}{\sigma_w}\right)^{-1} \tag{A3}$$

Handy (1990) suggested two additional bounding limits, the equations for which are nearly identical to the Voigt and Reuss bounds (see discussion in Ji et al. (2001)), with minor modification to the Reuss bound:

$$\sigma_c = \sigma_w \phi_w + \sigma_s \phi_s \tag{A4}$$

where $x = (1 - \sigma_w/\sigma_s)$. However, when Eqs. (A3) and (A5) are plotted, they are virtually indistinguishable.

Eqs. (A1)–(A4) are appropriate for describing theoretical bounds of aggregate strength for linear viscous materials, but most rock-forming minerals are thought to follow non-linear, strain-rate and temperature dependent flow laws of the form:

$$\dot{\varepsilon} = A\sigma^n \exp^{\left(\frac{-Q}{RT}\right)} \tag{A4a}$$

or

$$\sigma = \left(\frac{\dot{\varepsilon}}{A\exp^{\left(\frac{-Q}{RT}\right)}}\right)^{\frac{1}{n}} \tag{A4b}$$

where A is a pre-exponential material constant, n is the stress exponent (typically on the order of 3), Q is the activation energy for a particular deformation mechanism, R is the gas constant, and T is temperature in Kelvin (e.g. Tullis et al., 1991). Using a combination of empirical and numerical experiments, Tullis et al. (1991) derived the following relationships for the power-law equation variables for two-phase aggregates:

$$n_a = 10^{(\phi_1 \log n_1 + \phi_2 \log n_2)} \tag{A5}$$

$$Q_a = \frac{Q_2(n_a - n_1) - Q_1(n_a - n_2)}{n_2 - n_1} \tag{A6}$$

$$A_a = 10^{\left[(\log A_2(n_a - n_1) - \log A_1(n_a - n_2)\right]/[n_2 - n_1]} \tag{A7}$$

which, when applied to numerical and empirical experimental results, yielded good fits for the strength-volume fraction trends of two-phase aggregates at low volume fractions of the strong phase (Tullis et al., 1991) (Fig. 1).

Two equations are used in Fig. 1 that demonstrates the influence of particle shape on the strength trend (Tharp, 1983; Treagus, 2002). Tharp (1983) introduced a geometric factor, k, which accounts for spherical ($k = 0.98$) to elliptical ($k = 3.8$) inclusions:

$$\sigma_a = \sigma_s(1 - k\phi_w) \tag{A8}$$

Eq. (A8) is only applicable for rounded inclusions, and is only strictly applicable if the volume fraction of the weak phase is less than 0.2 (e.g. Handy, 1990). Treagus (2002) used two-dimensional analytical models to derive the following equation describing the effects of different shaped inclusions on the strength of a composite:

$$\sigma* = \frac{-\left[(m-p) - \alpha(m-1)(1+p)\right] + \sqrt{\left[(m-p) - \alpha(m-1)(1+p)\right]^2 + 4pm}}{2p} \tag{A9}$$

where $\sigma*$ is the normalized strength (formulated as a viscosity contrast by Treagus (2002)), m is the strength contrast between the two phases, p is a shape factor and α is the volume fraction of the clast. Treagus (2002) experimented with circular ($p = 1$), rhombohedral ($p \sim 1$), square ($p = 9$), and elliptical ($p = 2.6$) clasts and determined that square inclusions had the largest effect on the aggregate strength, which is consistent with finite element models presented by Tullis et al. (1991).

References

Allen, T.T., 1992. Migmatite systematics and geology, Carter Dome-Wild River region, White Mountains, New Hampshire. PhD Thesis, Dartmouth College.

Allmendinger, R.W., 2002. StereoWin for Windows: ftp://www.geo.cornell.edu/pub/rwa.

Arzi, A.A., 1978. Critical phenomena in the rheology of partially melted rocks. Tectonophysics 44, 173–184.

Barnes, J.D., Selverstone, J., Sharp, Z.D., 2004. Interactions between serpentinite devolatization, metasomatism and strike-slip strain localization during deep-crustal shearing in the Eastern Alps. Journal of Metamorphic Geology 22, 283–300.

Bell, T.H., Hayward, N., 1991. Episodic metamorphic reactions during orogenesis: the control of deformation partitioning on reaction sites and reaction duration. Journal of Metamorphic Geology 9, 619–640.

Bell, T.H., Ham, A.P., Kim, H.S., 2004. Partitioning of deformation along an orogen and its effects on porphyroblast growth during orogenesis. Journal of Structural Geology 26, 825–845.

Bons, P.D., Urai, J.L., 1994. Experimental deformation of two-phase rock analogues. Materials Science and Engineering A175, 221–229.

Bradley, D.C., 1983. Tectonics of the Acadian Orogeny in New England and adjacent Canada. Journal of Geology 91, 381–400.

Bradley, D.C., Tucker, R.D., Lux, D.R., Harris, A.G., McGregor, D.C., 2000. Migration of the Acadian orogen and foreland basin across the Northern Appalachians. United States Geological Survey Professional Paper 1624, 49pp.

Brodie, K.H., Rutter, E.H., 1985. On the relationship between deformation and metamorphism, with special reference to the behavior of basic rocks. In: Thompson, A.B., Rubie, D.C. (Eds.), Metamorphic Reactions: Kinetics, Textures and Deformation Advances in Physical Geochemistry 4, pp. 138–179.

Brodie, K.H., Rutter, E.H., 1987. The role of transiently fine-grained reaction products in syntectonic metamorphism: natural and experimental examples. Canadian Journal of Earth Sciences 24, 556–564.

Brown, M., Solar, G.S., 1998. Shear zones systems and melts: feedback relations and self-organization in orogenic belts. Journal of Structural Geology 20, 211–227.

Bucher, K., Frey, M., 1994. Petrogenesis of Metamorphic Rocks. Springer-Verlag, Berlin.

Carminati, E., Siletto, G.B., 1997. The effects of brittle–plastic transitions in basement-involved foreland belts: the Central Southern Alps case (N. Italy). Tectonophysics 280, 107–123.

Chapple, W.M., 1968. A mathematical theory of finite-amplitude rock-folding. GSA Bulletin 79, 47–68.

Chapple, W.M., 1969. Fold shape and rheology: the folding of an isolated viscous-plastic layer. Tectonophysics 7, 97–116.

Chen, W., Molnar, P., 1983. Focal depths of intracontinental and intraplate earthquakes and their implication for the thermal and mechanical properties of the lithosphere. Journal of Geophysical Research 88, 4183–4214.

De Bresser, J.H.P., Ter Heege, J.H., Spires, C.J., 2001. Grain size reduction by dynamic recrystallization: can it result in major rheologic weakening? International Journal of Earth Sciences 90, 28–45.

DeCelles, P.G., 2004. Late Jurassic to Eocene evolution of the Cordilleran thrust belt and foreland basin system, western USA. American Journal of Science 304, 105–168.

Della Vedova, B., Lucaseau, F., Pasquale, V., Pellis, G., Verdova, M., 1995. Heat flow in the tectonic provinces crossed by the southern segment of the European Geotraverse. Tectonophysics 244, 57–74.

Dieterich, J.H., 1969. Origin of cleavage in folded rocks. American Journal of Science 267, 155–165.

Dominic, J., McConnell, D.A., 1994. The influence of structural lithic units in fault-related folds, Seminoe Mountains, Wyoming, USA. Journal of Structural Geology 16, 769–779.

Duva, J.M. 1984. A self-consistent analysis of the stiffening effect of rigid inclusions on a power-law material. Journal of Engineering Materials and Science, 106, 317–321.

Eusden, J.D., Garesche, J.M., Johnson, A.H., Maconochie, J., Peters, S.P., O'Brien, J.B., Widmann, B.L., 1996. Stratigraphy and ductile structure of the Presidential Range, New Hampshire: tectonic implications for the Acadian Orogeny. GSA Bulletin 108, 417–437.

Eusden, J.D., Guzofski, C.A., Robinson, A.C., Tucker, R.D., 2000. Timing of the Acadian Orogeny in Northern New Hampshire. Journal of Geology 108, 219–232.

Farver, J.R., Yund, R.A., 1999. Oxygen bulk diffusion measurements and TEM characterization of a natural mylonite: implications for fluid transport in mica-bearing rocks. Journal of Metamorphic Geology 17, 669–683.

Farver, J.R., Yund, R.A., 2000. Silicon diffusion in a natural quartz aggregate: constraints on solution-transfer diffusion creep. Tectonophysics 325, 193–205.

Fletcher, R.C., 1979. The shape of single-layer folds at small but finite amplitude. Tectonophysics 60, 77–87.

Freuh-Green, G.L., 1994. Interdependence of deformation, fluid infiltration and reaction progress recorded in eclogitic metagranitoids (Sesia Zone, Western Alps). Journal of Metamorphic Geology 12, 327–343.

Gardien, V., Thompson, A.B., Grujic, D., Ulmer, P., 1995. Experimental melting of biotite + plagioclase + quartz + muscovite assemblages and implications for crustal melting. Journal of Geophysical Research 100, 15581–15591.

Gay, N.C., 1968a. Pure shear and simple shear deformation of inhomogeneous viscous fluids I: Theory. Tectonophysics 5, 211–234.

Gay, N.C., 1968b. Pure shear and simple shear deformation of inhomogeneous viscous fluids II: The determination of the total finite strain in a rock from objects such as deformed pebbles. Tectonophysics 5, 295–302.

Gay, N.C., 1976. The change of shape of a viscous ellipsoidal region embedded in a slowly deforming matrix having a different viscosity: a discussion. Tectonophysics 35, 403–407.

Groome, W.G., Johnson, S.E, Koons, P.O., in press. The effects of porphyroblast growth on the effective viscosity of metapelitic rocks: implications for the strength of the middle crust. Journal of Metamorphic Geology.

Gross, M.R., Guiterrez-Alonso, G., Bai, T., Wacker, M.A., Collinsworth, K.B., 1997. Influence of mechanical stratigraphy and kinematics on fault scaling problems. Journal of Structural Geology 19, 171–183.

Hacker, B.R., Peacock, S.M., Abers, G.A., Holloway, S.D., 2003. Subduction Factory 2: are intermediate-depth earthquakes in subducting slabs linked to metamorphic dehydration reactions? Journal of Geophysical Research 108 (B1), 2030. doi:10.1029/2001JB001129.

Handy, M.R., 1990. The solid-state flow of polymineralic rocks. Journal of Geophysical Research 95, 8647–8661.

Handy, M.R., Mulch, A., Rosenau, M., Rosenberg, C.L., 2001. The role of fault zones and melts as agents of weakening, hardening and differentiation of the continental crust: a synthesis. In: Hodslworth, R.E., Strachen, R.A., Magloughlin, J.F., Knipe, R.J. (Eds.), The Nature and Tectonic Significance of Fault Zone Weakening Geological Society, London, Special Publications 186, pp. 305–332.

Hatch, N.L., Moench, R.H., Lyons, J.B., 1983. Silurian–Lower Devonian stratigraphy of eastern and south-central New Hampshire: extensions from Western Maine. American Journal of Science 283, 739–761.

Henderson, J.R., Wright, T.O., Henderson, M.N., 1986. A history of cleavage and folding: an example from the Goldenville Formation, Nova Scotia. GSA Bulletin 97, 1354–1366.

Hippertt, J., Lana, C., Takeshita, T., 2001. Deformation partitioning during folding of banded iron formation. Journal of Structural Geology 23, 819–834.

Hirth, G., Teyssier, C., Dunlap, W.J., 2001. An evaluation of quartzite flow laws based on comparisons between experimentally and naturally deformed rocks. International Journal of Earth Sciences 90, 77–87.

Hobbs, B.E., Means, W.D., Williams, P.F., 1982. The relationship between foliation and strain: an experimental investigation. Journal of Structural Geology 4, 411–428.

Hollister, L.S., Crawford, M.L., 1986. Melt-enhanced deformation: a major tectonic process. Geology 14, 558–561.

Holt, W.E., Chamot-Rooke, N., Le Pichon, X., Haines, A.J., Shen-Tu, B., Ren, J., 2000. Velocity fields in Asia inferred from Quaternary fault slip rates and Global Positioning System observations. Journal of Geophysical Research 105, 19185–19209.

Hudleston, P.J., Holst, T.B., 1984. Strain analysis and fold shape in a limestone layer and implications for layer rheology. Tectonophysics 106, 321–347.

Hudleston, P.J., Lan, L., 1995. Rheological information from geological structures. Pure and Applied Geophysics 145, 605–620.

Jamieson, R.A., Beaumont, C., Nguyen, M.H., Lee, B., 2002. Interaction of metamorphism, deformation and exhumation in large convergent orogens. Journal of Metamorphic Geology 20, 9–24.

Ji, S., 2004. A generalized mixture rule for estimating the viscosity of solid-liquid suspensions and mechanical properties of polyphase rocks and composite materials. Journal of Geophysical Research 109. doi:10.1029/2004/JB003124.

Ji, S., Xia, B., 2002. Rheology of Polyphase Earth Materials. Polytechnic Press International, Montreal.

Ji, S., Zhao, P., 1993. Flow laws of multiphase rocks calculated from experimental data on the constituent phases. Earth and Planetary Science Letters 117, 181–187.

Ji, S., Wang, Z., Wirth, R., 2001. Bulk flow strength of forsterite–enstatite composites as a function of forsterite content. Tectonophysics 341, 69–93.

Jin, Z.M., Zhang, J., Green III., H.W., Jin, S., 2001. Eclogite rheology: implications for subducted lithosphere. Geology 29, 667–670.

Johnson, S.E., 1999. Porphyroblast microstructures: a review of current and future trends. American Mineralogist 84, 1711–1726.

Johnson, T.E., Hudson, N.F.C., Droop, G.T.R., 2001. Partial melting in the Inzie Head gneisses: the role of water and a petrogenetic grid in the KFMASH applicable to anatectic pelitic migmatites. Journal of Metamorphic Geology 19, 99–118.

Johnson, S.E., Vernon, R.H., Upton, P. 2004. Foliation development and the progressive strain-rate partitioning in the crystallizing carapace of a tonalite pluton: microstructural evidence and numerical modeling. Journal of Structural Geology, 26, 1845–1865.

Jordan, P., 1987. The deformational behaviour of bimineralic limestone–halite aggregates. Tectonophysics 135, 185–197.

Jordan, P., 1988. The rheology of polymineralic rocks—an approach. Geologische Rundschau 77, 285–294.

Kanagawa, K., 1993. Competence contrasts in ductile deformation as illustrated from naturally deformed chert-mudstone layers. Journal of Structural Geology 15, 865–885.

Keller, L.M., Abart, R., Stunitz, H., De Capitani, C., 2004. Deformation, mass transfer and mineral reactions in an eclogite facies shear zone in a polymetamorphic metapelite (Monte Rosa nappe, western Alps). Journal of Metamorphic Geology 22, 97–118.

Kenis, I., Urai, J.L., van der Zee, W., Sintubin, M., 2004. Mullions in the High-Ardenne Slate Belt (Belgium): numerical model and parameter sensitivity analysis. Journal of Structural Geology 26, 1677–1692.

Kenis, I., Urai, J.L., van der Zee, W., Hilgers, C., Sintubin, M., 2005. Rheology of fine-grained siliciclastic rocks in the middle crust: evidence from structural and numerical analysis. Earth and Planetary Sciences Letters 233, 351–360.

Klepeis, K.A., Clarke, G.L., Gehrels, G., Vervoort, J., 2004. Processes controlling vertical coupling and decoupling between the upper and lower crust of orogens: results from Fjordland, New Zealand. Journal of Structural Geology 26, 765–791.

Kohlstedt, D.L., Evans, B., Mackwell, S.J., 1995. Strength of the lithosphere: constraints imposed by laboratory experiments. Journal of Geophysical Research 100, 17587–17602.

Koons, P.O., 1989. The topographic evolution of collisional mountain belts: a numerical look at the Southern Alps, New Zealand. American Journal of Science 289, 1041–1069.

Koons, P.O., 1995. Modeling the topographic evolution of collisional belts. Annual Reviews of Earth and Planetary Sciences 23, 375–408.

Koons, P.O., Rubie, D.C., Frueh-Green, G., 1987. The effects of disequilibrium and deformation on the mineralogical evolution of quartz diorite during metamorphism in the eclogite facies. Journal of Petrology 28, 679–700.

Koons, P.O., Zeitler, P.K., Chamberlain, C.P., Craw, D., Melzer, A.S., 2002. Mechanical links between erosion and metamorphism in Nanga Parbat, Pakistan Himalaya. American Journal of Science 302, 749–773.

Kuhni, A., Pfiffner, O.A., 2001. Drainage patterns and tectonic forcing: a model study for the Swiss Alps. Basin Research 13, 169–197.

Kugel, K.L., 2004. Late Acadian D4 shortening, Chandler Ridge, Mount Washington, New Hampshire. BS Honors Thesis, Bates College.

Lagoeiro, L., Hippert, J., Lana, C. 2003. Deformation partitioning during folding and transposition of quartz layers. Tectonophysics, 361, 171–186.

Lisle, R.J., Rondeel, H.E., Doorn, D., Brugge, J., van de Gaag, P., 1983. Estimation of viscosity contrast and finite strain from deformed elliptical inclusions. Journal of Structural Geology 5, 603–609.

Maggi, A., Jackson, J.A., McKenzie, D., Priestley, K., 2000. Earthquake focal depths, effective elastic thickness and the strength of the continental lithosphere. Geology 28, 495–498.

Miller, R.B., Paterson, S.R., 2001. Influence of lithological heterogeneity, mechanical anisotropy and magmatism on the rheology of an arc, North Cascades, Washington. Tectonophysics 342, 351–370.

Moecher, D.P., Wintsch, R.P., 1994. Deformation-induced reconstitution and local resetting of mineral equilibria in polymetamorphic gneisses: tectonic and metamorphic implications. Journal of Metamorphic Geology 12, 523–538.

Molnar, P., Tapponnier, P., 1981. A possible dependence of tectonic strength on the age of the crust in Asia. Earth and Planetary Science Letters 52, 107–114.

Moore, J.C., Saffer, D., 2001. Updip limit of the seismogenic zone beneath the accretionary prism of southwest Japan: an effect of diagenetic to low-grade metamorphic processes and increasing effective stress. Geology 29, 183–186.

Panien, M., Schreurs, G., Pfiffner, A., 2005. Sandbox experiments on basin inversion: testing the influence of basin orientation and basin fill. Journal of Structural Geology 27, 433–445.

Passchier, C.W., Trouw, R.A.J., 1996. Microtectonics. Springer, Berlin.

Patino Duce, A., Johnston, A.D., 1991. Phase equilibria and melt productivity in the pelitic system: implications for the origin of peraluminous granitoids and aluminous granulites. Contributions to Mineralogy and Petrology 107, 202–218.

Petrini, K., Connolly, J.A.D., Podladchikov, Y.Y., 2001. A coupled petrological-tectonic model for sedimentary basin evolution: the influence of metamorphic reactions on basin subsidence. Terra Nova 13, 354–359.

Poirier, J.P., 1982. On transformation plasticity. Journal of Geophysical Research 87, 6791–6797.

Roberts, D., Stromgard, K., 1972. A comparison of natural and experimental strain patterns around hinge zones. Tectonophysics 14, 105–120.

Rodda, C.I., 2005. Early and Late Acadian strain partitioning: L1 lineation and F4 folding: Mt. Madison, New Hampshire. BS Honors Thesis, Bates College.

Rubie, D.C., 1983. Reaction-enhanced ductility: the role of solid-solid univariant reactions in deformation of the crust and mantle. Tectonophysics 96, 331–352.

Rubie, D.C., 1986. The catalysis of mineral reactions by water and restrictions on the presence of aqueous fluid during metamorphism. Mineralogical Magazine 50, 399–415.

Schlunegger, F., Hinderer, M., 2001. Crustal uplift in the Alps: why drainage pattern matters. Terra Nova 13, 425–432.

Sengupta, S., 1997. Contrasting fabrics in deformed dykes and host rocks: natural examples and a simplified model. In: Sengupta, S. (Ed.), Evolution of Geological Structures in Micro- to Macro-scales. Chapman and Hall, London, pp. 293–318.

Shackleton, J.R., Cooke, M.L., Sussman, A.J., 2005. Evidence for temporally changing mechanical stratigraphy and effects on joint-network architecture. Geology 33, 101–104.

Shea, W.T., Kronnenburg, A.K., 1993. Strength and anisotropy of foliated rocks with varied mica content. Journal of Structural Geology 15, 1097–1121.

Smith, R.B., 1975. Unified theory of the onset of folding, boudinage and mullion structure. GSA Bulletin 86, 1601–1609.

Smith, R.B., 1977. Formation of folds, boudinage and mullions in non-Newtonian materials. GSA Bulletin 88, 312–320.

Steffen, K., Selverstone, J., Brearley, A., 2001. Episodic weakening and strengthening during synmetamorphic deformation in a deep-crustal shear zone in the Alps. In: Holdsworth, R.E., Strachen, R.A., Magloughlin, J.R., Knipe, R.J. (Eds.), The Nature and Tectonic Significance of Fault Zone Weakening Geological Society, London, Special Publications 186, pp. 141–156.

Stunitz, H., Tullis, J., 2001. Weakening and strain localization produced by syn-deformational reaction of plagioclase. International Journal of Earth Sciences 90, 136–148.

Takeda, Y., 1998. Flow in rocks modeled as multiphase continua: application to polymineralic rocks. Journal of Structural Geology 11, 1569–1578.

Takeda, Y., Obata, M., 2003. Some comments on the rheologically critical melt percentage. Journal of Structural Geology 25, 813–818.

Talbot, C.J., 1999. Can field data constrain rock viscosities? Journal of Structural Geology 21, 949–957.

Tenthorey, E., Cox, S.F., 2003. Reaction-enhanced permeability during serpentine dehydration. Geology 31, 921–924.

Tharp, T.M. 1983. Analogies between the high-temperature deformation of polyphase rocks and the mechanical behavior of porous powder metals. Tectonophysics, 96, 1–11.

Tobisch, O.T., Barton, M.D., Vernon, R.H., Paterson, S.R., 1991. Fluid-enhanced deformation: transformation of granitoids to banded mylonites, western Sierra Nevada, California and southeastern Australia. Journal of Structural Geology 13, 1137–1156.

Treagus, S.H., 1983. A theory of finite strain variation through contrasting layers, and its bearing on cleavage refraction. Journal of Structural Geology 5, 351–368.

Treagus, S.H., 1988. Strain refraction in layered systems. Journal of Structural Geology 10, 517–527.

Treagus, S.H., 1999. Are viscosity ratios measureable from cleavage refraction? Journal of Structural Geology 21, 895–901.

Treagus, S.H., 2002. Modelling the bulk viscosity of two-phase mixtures in terms of clast shape. Journal of Structural Geology 24, 57–76.

Treagus, S.H., Treagus, J.E., 2002. Studies of strain and rheology of conglomerates. Journal of Structural Geology 24, 1541–1567.

Tucker, R.D., Osberg, P.H., Berry, H.N. IV. 2001. The geology of a part of Acadia and the nature of the Acadian orogeny across central and eastern Maine. American Journal of Science, 301, 205–260.

Tullis, J., Wenk, H.-R., 1994. Effect of muscovite on the strength and lattice preferred orientations of experimentally deformed quartz aggregates. Materials Science and Engineering A175, 209–220.

Tullis, T.E., Horowitz, F.G., Tullis, J., 1991. Flow laws of polyphase aggregates from end-member flow laws. Journal of Geophysical Research 96, 8081–8096.

Upton, P., Koons, P.O., Eberhart-Phillips, D., 2003. Extension and partitioning in an oblique subduction zone, New Zealand: Constraints from three-dimensional numerical modeling. Tectonics 22, 1068. doi:10.1029/2002TC001431.

Urai, J.L., Spaeth, G., Van Der Zee, W., Hilgers, C., 2001. Evolution of mullion (boudin) structures in the Variscan of the Ardennes and Eifel. Journal of the Virtual Explorer 3, 1–16.

Van Staal, C.R., Dewey, J.F., Mac Niocaill, C., McKerrow, W.S., 1998. The Cambrian–Silurian tectonic evolution of the northern Appalachians and British Caledonides: history of a complex, west and southwest Pacific-type segment of Iapetus. In: Blundell, D.J., Scott, A.C. (Eds.), Lyell: The Past is the Key to the Present Geological Society, London, Special Publication 143, pp. 199–242.

Vernon, R.H., 2004. A Practical Guide to Rock Microstructures. Cambridge University Press.

Viola, G., Mancktelow, N.S., 2005. From XY tracking to buckling: axial plane cleavage fanning and folding during progressive deformation. Journal of Structural Geology 27, 409–417.

Wall, E.R., 1988. The occurrence of staurolite and its implication for polymetamorphism in the Mt. Washington area, New Hampshire. MS Thesis, University of Maine.

Willet, S.D., Fisher, D., Fuller, C., En-Cho, Y., Chia-Yu, L., 2003. Erosion rates and orogenic wedge kinematics in Taiwan inferred from fission-track thermochronology. Geology 31, 945–948.

Williams, C.A., Connors, C., Dahlen, F.A., Price, E.J., Suppe, J., 1994. Effect of brittle–ductile transition on the topography of compressive mountain belts on Earth and Venus. Journal of Geophysical Research 99, 19947–19974.

Zeitler, P.K., Chamberlain, C.P., Smith, H.A., 1993. Synchronous anatexis, metamorphism and rapid denudation at Nanga Parbat (Pakistan Himalaya). Geology 21, 347–350.